Supplemental data

Supplemental Figures

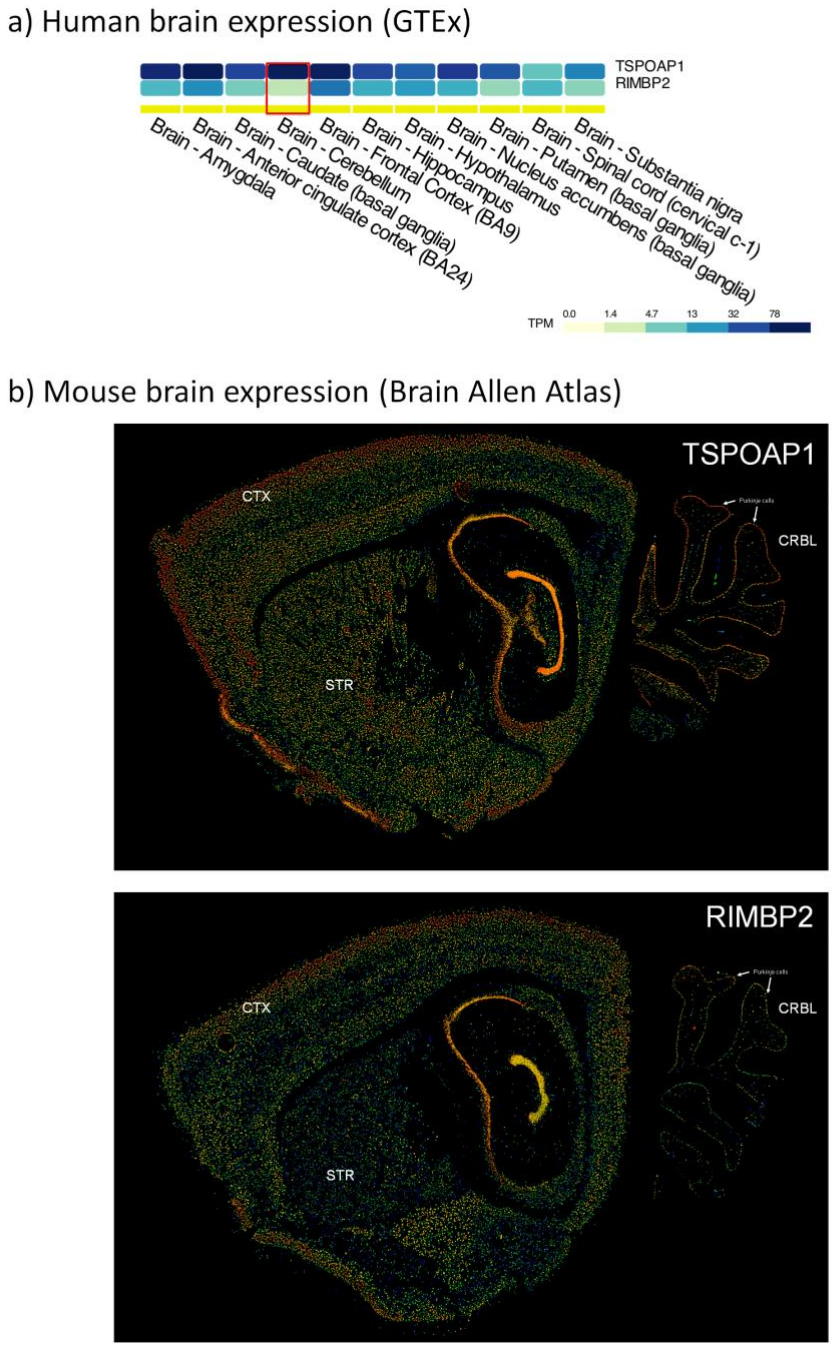

Suppl. Figure 1. Expression patterns of RIMBPs in human and mouse brain.
A. Expression in the human brain. Levels of *TSPOAP1/*RIMBP1 and *RIMBP2* mRNA expression levels in eleven adult human brain regions (source: GTEx, see Web Resources). These dataset levels were generated with Illumina TrueSeq RNA sequencing and Affymetrix Human Gene 1.1 ST Expression Array (V3; 837 samples) and tissue originating from nearly 1000 donors. Gene and transcript expression levels on the GTEx Portal are shown in Transcripts Per Million (TPM).
B. Expression in mouse brain. *TSPAOPA1/* RIMBP1 and *RIMBP2* expression in the mouse brain in sagittal sections. Images were obtained from the Allen Mouse Brain Atlas (©2015 Allen Institute for Brain Science). Expression intensity is color-coded and ranges from low (blue) to moderate (green, yellow) to high (red) intensity.

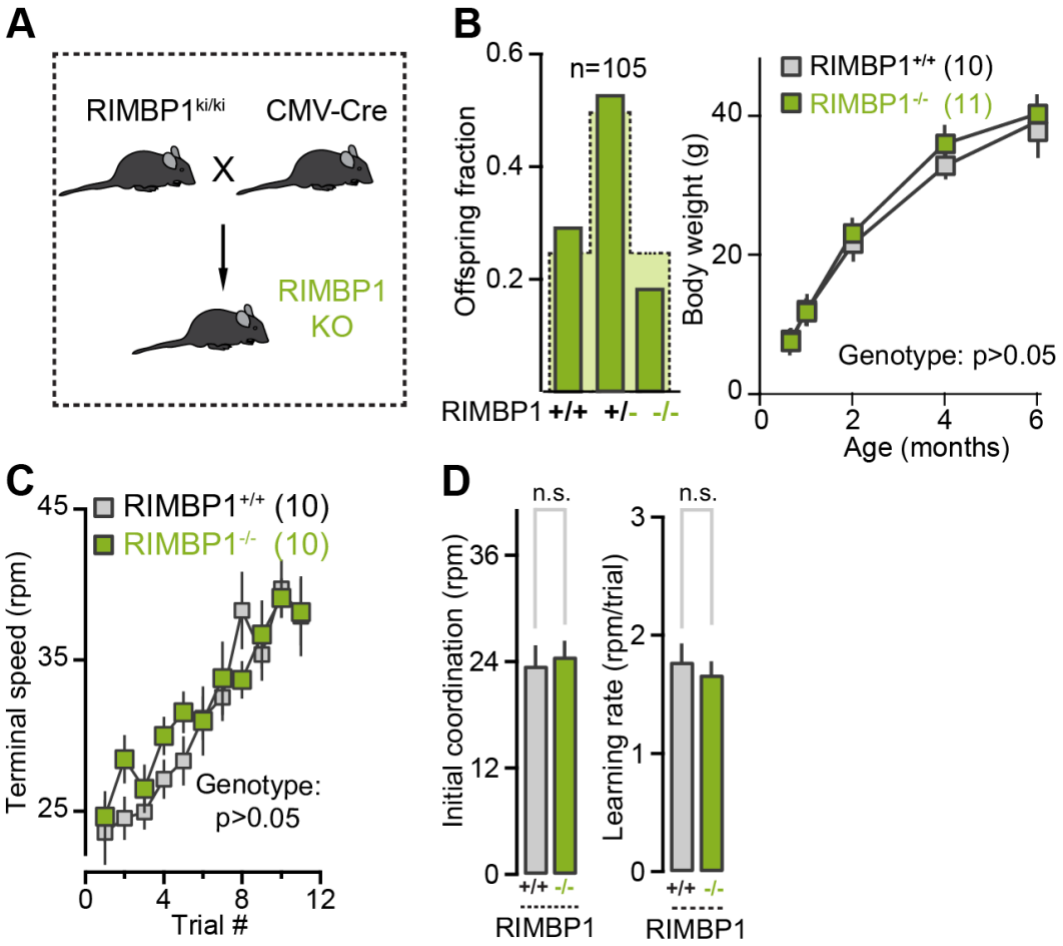

Suppl. Figure 2. RIMBP1 constitutive knock-out mice.

A. Schematic of crosses used to generate constitutive RIMBP1 KO and littermates control mice.

B. Left. Breeding offspring ratios resulting from RIMBP1 heterozygotes matings (105 mice were analyzed in total). Expected Mendelian ratios are shown by the dotted line. Right. Body weight of RIMBP1 WT and RIMBP1 KO mice.

C. Accelerating rota-rod test. Terminal speed as a function of trial number in RIMBP1 control and mutant mice.

D. Accelerating rotarod test. Left, summary graph of averaged initial motor coordination (terminal speed on day1, session1). Right, learning rate (slope of linear function from terminal speed vs trial # graph) in control and littermates KO mice.

Data are mean±SEM. Number of experiments: **C**, **D**. 10 WT, 10 KO. Statistical analysis was assessed by ANOVA (**C**) and Student's t-test (**D**); $^{*}p < 0.05$, $^{**}p < 0.01$, and $^{***}p < 0.001$; n.s., non-significant.

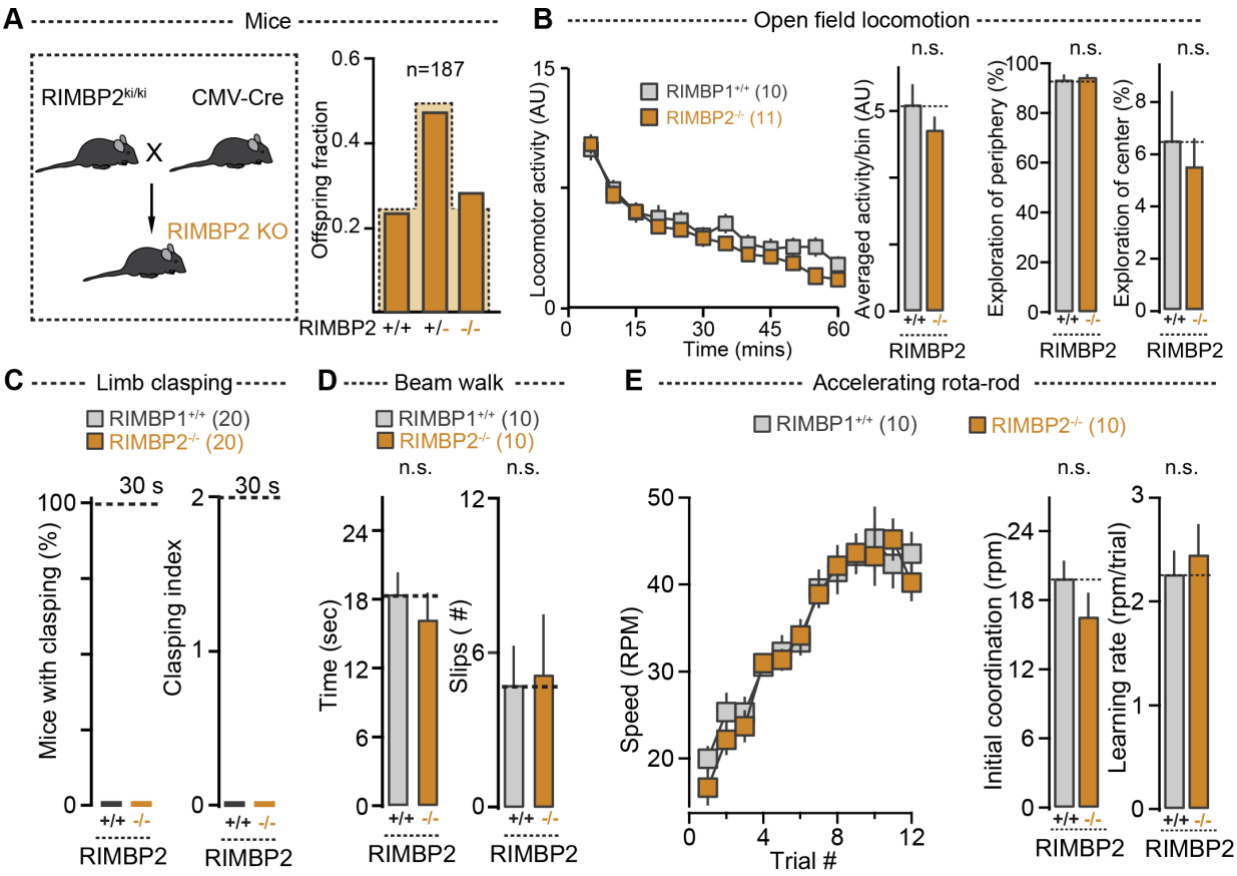

Suppl. Figure3. Motor performance of RIMBP2 constitutive knock-out mice.

A. Left, schematic of crosses used to generate constitutive RIMBP2 KO and littermates control mice. Right, breeding offspring ratios resulting from RIMBP2 heterozygotes matings (187 mice were analyzed in total). Expected Mendelian ratios are shown by the dotted line.

B. Open field locomotor activity. Left, locomotor activity as a function of time (bin width: 5 mins). Middle left, bar graph of total activity in RIMBP2 WT and RIMBP2 KO mice. Middle right, comparison of relative activity in the periphery (P) of the open field arena in control and mutant mice. Right, comparison of relative activity in the center (C) of the open field arena in control and mutant mice.

C. Limb-clasping test. Left, percentage of RIMBP2 WT and RIMBP2 KO mice displaying limb clasping in tail suspension test lasting 30 secs. Right, clasping index in control and mutant mice tail-suspended for 30 secs.

D. Beam-walk test. Left, summary graphs of total time to cross the beam. Right, summary graphs of total number of slips.

E. Accelerating rota-rod test. Left, terminal speed as a function of trial number in RIMBP2 control and mutant mice. Middle, summary graph of averaged initial motor coordination (terminal speed on day1, session1). Right, learning rate (slope of linear function from terminal speed vs trial # graph) in control and littermates KO mice.

Data are mean±SEM. Number of experiments: B, right: 10 WT, 11 KO; C: 20 WT, 20 KO; D: 10 WT, 10 KO; E: 10 WT, 10 KO. Statistical analysis was assessed by Student's t-test and ANOVA. $^{*}p < 0.05$, $^{**}p < 0.01$, and $^{***}p < 0.001$; n.s., non-significant.

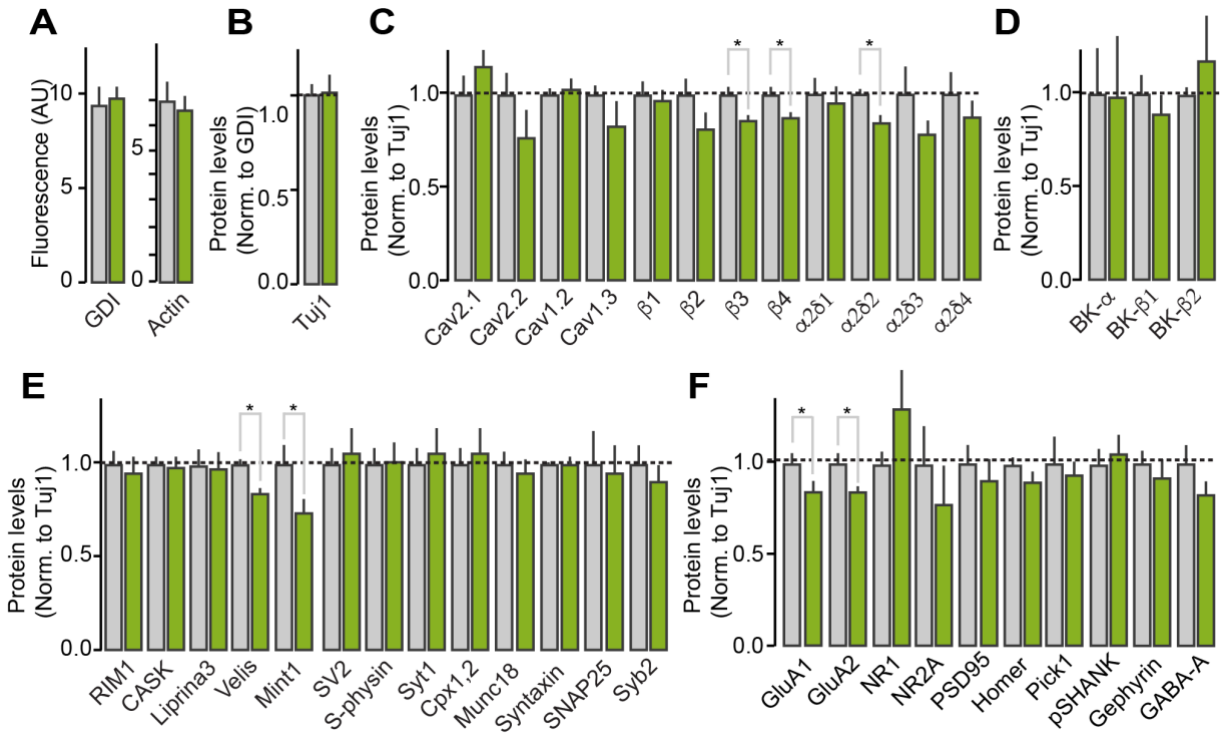

Suppl. Figure 4. Biochemical composition of the cerebellum upon deletion of RIMBP1.
A. Bar graphs summarizing the raw intensity of fluorescent signals arising from GDI and Actin after Western Blot analysis in RIMBP1 WT and KO cerebelli.
B. Summary graph showing Tuj1 signals normalized to GDI in RIMBP1 WT and KO cerebelli.
C. Summary graph of the levels of calcium-channel a-subunit, b-subunits, and a2d subunits in cerebelli from littermates RIMBP1 control and mutant mice.
D. Same as in **C** but BK-channels (a, b1, and b2).
E. Bar graphs showing the levels of several active zone, as well as of vesicle-associated proteins, SNAREs, and other presynaptic proteins that collaborate with SNAREs in synaptic vesicle fusion. All samples were obtained from cerebellar lysates from controls and RIMBP1 KO mice.
F. Summary graphs displaying the levels of several postsynaptic proteins and receptors for both excitatory and inhibitory neurotransmitters. Detailed information of the antibodies and dilution used can be found in the supplementary material.
Data are mean±SEM. Number of experiments (mice/sections): **A:** 12 WT, 12 KO, **B**: 10 WT, 10 KO, **C:** 7WT, 8 KO**; D**: 9 WT, 8 KO; **E**: 8 WT, 8 KO; **F:** 8 WT, 8 KO. Statistical analysis was assessed by Student's t-test. $^{*}p < 0.05$ and $^{***}p < 0.001$; n.s., non-significant.

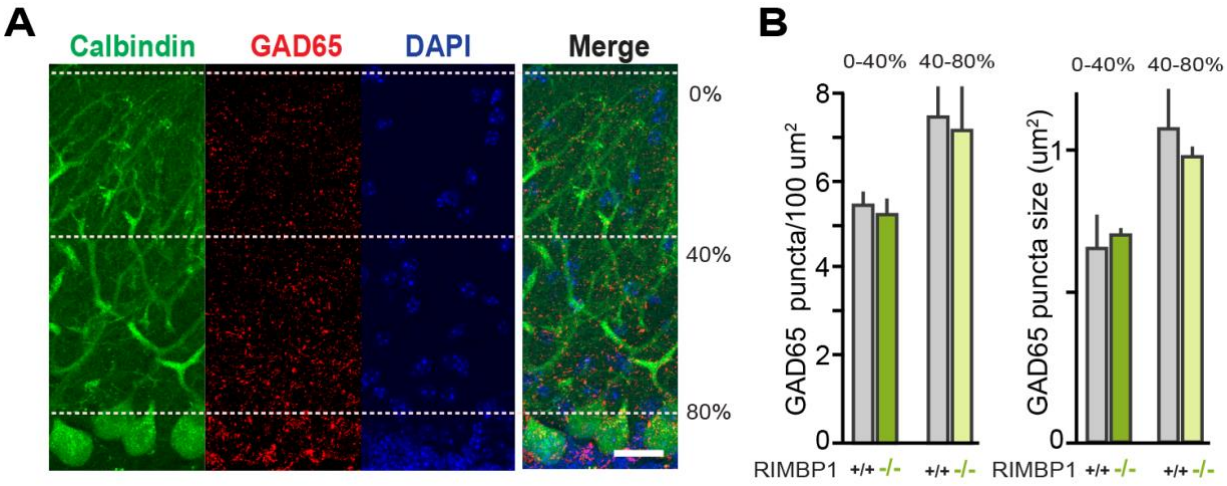

Suppl. Figure 5. Cerebellar inhibitory synapses in RIMBP1 knock-out mice.
A. Representative confocal images of cerebellar sections from a RIMBP1-WT mouse stained with antibodies anti-Calbindin (green, to label Purkinje cells), anti-GAD65 (red, to visualize inhibitory terminals), and with DAPI (blue, cell nuclei). Scale bar: 20 μm.
B. Summary graphs of GAD65 cluster density (puncta/100um^2, left) and GAD65 cluster size (right) in the outermost (0-40%) and innermost (40-80%) dendritic domains of Purkinje cells.

Data are mean±SEM. Number of experiments (mice/sections): 3/24 WT, 3/27 KO. Statistical analysis was assessed by Student's t-test. $^{*}p < 0.05$ and $^{***}p < 0.001$; n.s., non-significant.

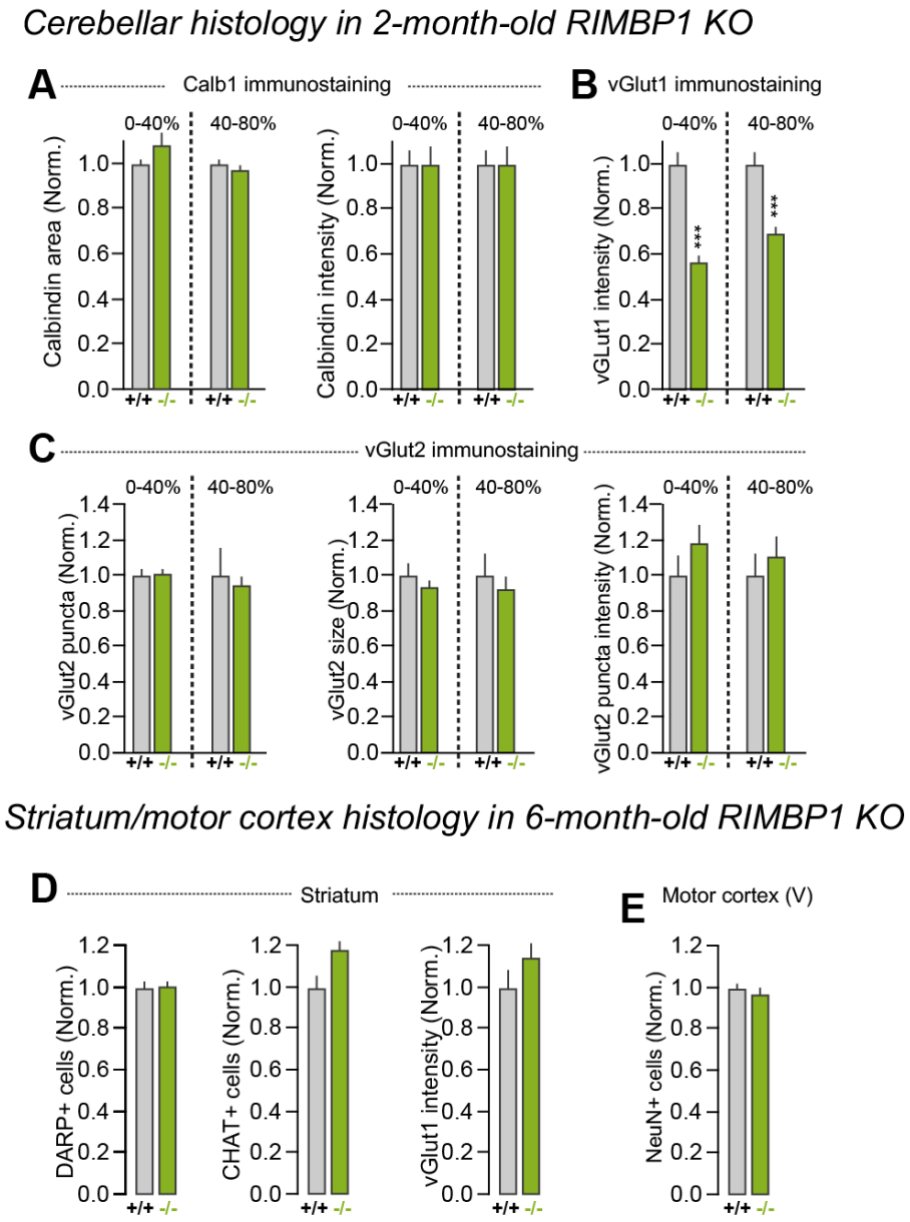

Suppl. Figure 6. Histological analysis of circuits involved in motor control in RIMBP1 knock-out mice.

A-C. Organization of the cerebellum in 2-month-old RIMBP1 WT (grey) and KO (green) mice. **A**. Left. Area covered by calbindin signal in the cerebellar cortex. Right. Intensity of Calbindin signals. **B**. Intensity of vGlut1 signals in the cerebellar cortex. **C**. vGlut2 signal in the cerebellar cortex. Left. Puncta number. Middle. Puncta size. Right. Puncta intensity. **D-E**. Structural integrity of the striatum and motor cortex in RIMBP1 WT (grey) and KO (green) mice. **D**. Summary of the number of DARP- and CHAT-positive cells and of the intensity of vGlut1-containing nerve terminals in the striatum of RIMBP1 KO mice. **E**. Number of NeuN-positive cells in the frontal motor cortex (layer 5).

Data are mean±SEM. Number of experiments (mice/sections): **A**: 2/24 WT, 2/24 KO. **B**: 2/24 WT, 2/24 KO. **C:**2/24 WT, 2/24 KO. **D**: 3/36 WT, 3/36 KO. **E**: 3/36 WT, 3/36 KO. Statistical analysis was assessed by Student's t-test. $^{*}p < 0.05$ and $^{***}p < 0.001$; n.s., non-significant.

Supplemental tables

Supplemental table 1. Standard quality metrics of whole-exome sequencing in families with *TSPOAP1* pathogenic variants

Sample ID	MEAN_TARGET_COVERAGE (reads)	PCT_TARGET_BASES_2X (%)	PCT_TARGET_BASES_10X (%)	PCT_TARGET_BASES_20X (%)
A.II-1	61.78	98.79	95.53	87.64
A.II-2	44.68	98.87	92.25	76.30
A.II-3	44.65	98.29	86.43	67.82
A.I-1	27.07	97.72	81.94	54.91
A.I-2	98.04	99.23	97.67	94.34
B.II-1	54.85	99.70	97.00	88.70
C.II-2	82.02	98.08	95.82	90.84
C.II-4	89.04	98.08	96.17	92.10

Supplemental table 2. Additional homozygous variants identified by whole-exome sequencing in families with *TSPOAP1* pathogenic variants

Chr. Position	Ref	Alt	Gene	AA Change	gnomAD MAF	Homozyg./hemizyg. count in gnomAD	CADD	SIFT	PolyPhen-2	Reasons to exclude pathogenicity
Family A										
14:20944705	A	G	*PNP*	NM_000270:c.815A>G, p.E272G	0.00006364	0	22.9	T	B	Not in disease-linked ROH; unaffected father is homozygote; normal purine metabolism
17:56403686	C	-	*TSPOAP1*	NM_004758:c.538delG, p.A180fs	0	0	NA	NA	NA	
Family B										
14:45403616	T	C	*KLHL28*	NM_017658:c.1045A>G, p.I349V	0.003643	4	15.24	T	B	Homozygous variants in gnomAD controls; in silico tools predict benign effect
14:105418115	C	T	*AHNAK2*	NM_138420:c.3673G>A, p.G1225S	0.0002529	18	10.13	T	B	Homozygous variants in gnomAD controls; in silico tools predict benign effect
17:56389733	G	A	*TSPOAP1*	NM_004758:c.2449C>T, p.Q817X	0	0	35	NA	NA	
17:56436023	G	A	*RNF43*	NM_017763:c.1114C> T, p.P372S	0.000234	0	10.13	T	B	In silico tools predict benign effect
17:59489823	C	A	*C17orf82*	NM_203425:c.487C>A, p.Q163K	0	0	14.42	T	D	In silico tools predict benign effect
X:101139206	T	C	*ZMAT1*	NM_001282400:c.680A>G, p.D227G	0.000009771	0	25.6	D	D	
X:135630910	G	A	*VGLL1*	NM_016267:c.377G>A, p.R126Q	0.0006238	55	2.726	T	B	Hemizygous variants in gnomAD controls; in silico tools predict benign effect
Family C										
8:36692371	T	C	*KCNU1*	NM_001031836:c.1280T>C, p.I427T	0.0001083	0	8.867	T	B	Affected siblings are both heterozygous; in silico tools predict benign effect
11:71174492	G	A	*NADSYN1*	NM_018161:c.278G>A, p.R93Q	0.00002123	0	23.1	T	B	Affected siblings are heterozygous (C-II.1) and wild-type (C-II.3)
17:56382759	C	T	*TSPOAP1*	NM_004758:c.5422G>A, p.G1808S	0.00001061	0	27.7	D	D	

Ref=reference allele; Alt=alternative allele; AA=amino acid; MAF=minor allele frequency; T=tolerated; B=benign; D=deleterious/damaging

Supplemental Movies

Video 1. Family A and Family B. Subject A-II.2. Exam shows severe dysarthria with mild orofacial dystonic movements with speech. There is elevation of the right shoulder and cervical dystonia with mild torticollis to the right. There is continuous dystonic posturing of bilateral upper extremities with finger flexion, wrist flexion and arm supination, particularly of left arm. Dystonic posturing worsens and there is muscle overflow when subjects is asked to hold arms extended in front of him as well as when attempting cerebellar maneuvers. There is no bradykinesia, but finger tapping movements are impaired by dystonic posturing of hands and there is also overflow to other forearm and arm muscles. Gait is narrow based, with bilateral foot inversion, worse on the right foot and dystonic posturing of bilateral upper extremities. Subject A-II.4. also shows whispering dysphonia suggestive of severe laryngeal dystonia. With speech, there are dystonic orofacial movements, also dystonic lingual movements. There is also left shoulder elevation and continuous dystonic posturing of right arm. Eye movement exam shows difficulty initiating saccades in all directions. There is bilateral dystonic posturing of upper extremities which worsen in severity when asked to hold arms extended in front of him and with cerebellar testing. Gait is narrow based, there is poor arm swing with dystonic posturing of right upper extremity with arm slightly abducted, extended wrist and fingers making a fist; there is slight foot eversion bilaterally and subject drags both feet when walking. The third segment shows subject B-II.1. At 17 years old there is generalized dystonia involving orofacial muscles, as well as upper extremities, with right arm abducted and held at the back and continuous dystonic posturing of left arm when attempting to use it, fingers are flexed and form a fist. Gait is narrow based, there is bilateral foot inversion, more prominent on the left, also with left leg circumduction; upper extremities are held away from his body with both hands making a fist. There cervical dystonia with anterocaput which is most noticeable towards the end of this segment. At 23 years old, gait has worsened, there is right foot inversion and knee flexion, both arms are held away from his body with hands making a fist, there is torticollis to the right, orofacial dystonia and blepharospasm. Orofacial and mandibular dystonia make tasks such as drinking or eating difficult, which is showcased in the last two segments.

Video 2. Family C. Subject C-II.4. On exam there is right shoulder elevation, mild right laterocollis, slight torticollis to the left and with slight retrocollis. Range of motion is full in all directions. Gait presents no abnormalities. Subject C-II.3. Examination shows a “no-no” head dystonic tremor. There is a mild, low frequency, high-amplitude postural tremor with upper limbs outstretched, most noticeable on index fingers. There is no evidence of dysarthria or bradykinesia. Gait shows good velocity and amplitude with slightly decreased arm swing bilaterally.

Video 3. Beam walking test in *TSPOAP1*/RIMBP1 wild-type (WT) and knock-out (KO) mice. Typical examples of beam crossing of a RIMBP-WT and a RIMBP1-KO mouse, showing a striking differences between genotypes in both the time to cross the beam as well as the total number of slips.

Video 4 Hindlimb clasping in *TSPOAP1*/RIMBP1 wild-type (WT) and knock-out (KO) mice. Side-by-side display of tail suspension test used to assess animal limb clasping.
Hindlimb clasping behaviour was consistently observed in RIMBP1-KO but not in RIMBP1-WT mice.

Video 5. Motor behavior comparison between *TSPOAP1*/RIMBP1 knock-out (KO) mice and TSPOAP1/RIMBP1 wild-type (WT). First segment shows motor behavior at baseline; RIMBP1-KO presents with mildly ataxic gait compared to RIMBP1-WT.

Second segment shows behavior 20 minutes after oxotremorine 0.01 mg/kg intraperitoneally. RIMBP1-KO displays severely limited ambulation with splayed posture and intermittent body and head jerks. At 60 minutes after oxotremorine injection, RIMBP1-KO still displays slowed movement with hindlimbs infrequently in a splayed posture.

Video 6. Examples of abnormal postures and movements in *TSPOAP1*/RIMBP1 knock-out (KO) mice. First segment shows a mouse with moderate impairment, with repetitive jerking of snout, limited ambulation, splayed posture and brief forelimb movements resembling the initial phases of grooming. The second segment shows severe impairment with a hunched posture and little movement, with frequent head jerks. The third segment shows a mouse with severe impairment, with limited movement and a sustained single raised paw.

Supplemental Table 3. List of antibodies used for Western blot analysis

Antigen	Antibody	Dilution
RIMBP-1 (RIM-Binding Protein-1)	316003	1:1000
RIMBP-2 (RIM-Binding Protein-2)	4193	1:1000
RIM 1 (RIM1 Central Domains)	R809	1:2000
RIM 2 (RIM2 C-Terminus)	T2795	1:250
Liprin α3	4396	1:5000
CASK	75-000	1:1000
Mint1	P932	1;1000
Veli1,2,3	T813	1:1000
Syntaxin 1	HPC-1	1:1000
SNAP 25	71.1	1:2000
Synaptobrevin 2	69.1	1:2500
Munc 18.1	K329	1:500
Complexin 1/2	L669	1:1000
Synaptotagmin 1	41.1	1:500
Synaptophysin	7.2	1:5000
SV 2	U1129	1:1000
Synapsin1,2	E28	1:500
Calbindin	CB-955	1:1000
GluA1	182003	1:1000
GluA2	182103	1:1000
NR1	75-272	1:1000
NR2A	75-288	1:1000
PSD95	73-028	1:1000
HOMER	160003	1:1000
PICK1	U58317	1:1000
SHANK	75-089	1:1000
Gephyrin	147111	1:1000
GABA-A	224211	1:1000
Ca^{2+}v1.2-α1C Voltage-Gated Channel	ACC-003	1:500

Ca^{2+}v1.3-α1D Voltage-Gated Channel	ACC-005	1:500
Ca^{2+}v2.1-α1A Voltage-Gated Channel	ACC-001	1:500
Ca^{2+}v2.2-α1B Voltage-Gated Channel	ACC-002	1:500
Ca^{2+}β1 Voltage-Gated Channel	ACC-106	1:500
Ca^{2+}β2 Voltage-Gated Channel	ACC-105	1:500
Ca^{2+}β3 Voltage-Gated Channel	ACC-008	1:500
Ca^{2+}β4 Voltage-Gated Channel	75-054	1:500
Ca^{2+}v-α2δ1 Voltage-Gated Channel	ACC-015	1:500
Ca^{2+}v-α2δ2 Voltage-Gated Channel	ACC-102	1:500
Ca^{2+}v-α2δ3 Voltage-Gated Channel	ACC-103	1:500
Ca^{2+}v-α2δ4 Voltage-Gated Channel	ACC-104	1:500
BK_{Ca}^{2+}- α	APC-021	1:500
BK_{Ca}^{2+}- β_1	APC-036	1:500
BK_{Ca}^{2+}- β_2	APC-034	1:500
TUJ1	T2200	1:4000
GDI	81.2	1:2000
NeuN	ABN78	1:1000
Myc	9B11	1:2000
HA	6E2	1:2000
GAPDH	MAB374	1:5000

Full unedited/uncropped blots0001 for Figure 3F
(area utilized in Figure 3F is highlighted in red)

Antigen: RIMBP1
Antibody: SYSY Cat#316003
Dilution: 1:1000

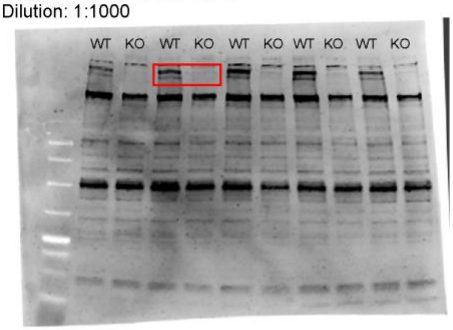

Antigen: RIMBP2
Antibody: 4193 (custom-Tom Südhof lab)
Dilution: 1:1000

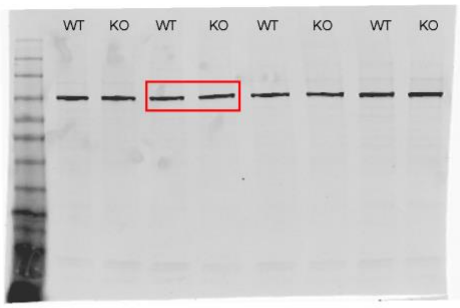

Antigen: Calb1 (calbindin)
Antibody: Abcam CB-955
Dilution: 1:1000

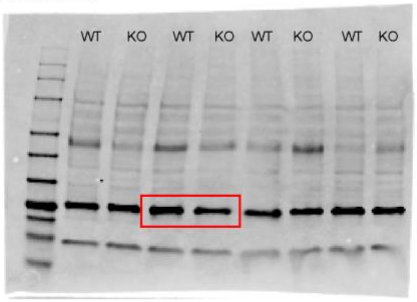

Antigen: Synapsin/Tuj1/GDI
Antibody: E28/T2200/81.2
Dilution: 1:500/1:400/1:2000

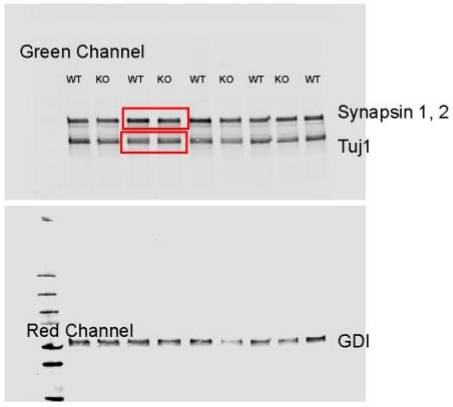

Full unedited/uncropped blots for Figure 4B
(area utilized in Figure 4B is highlighted in red)

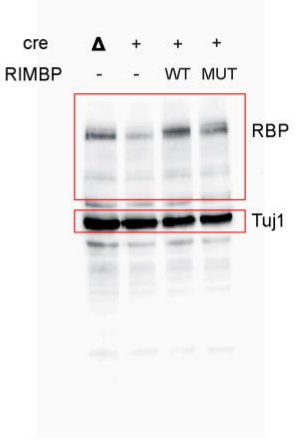

unedited/uncropped blots used in Figure 4F

HA-Cav2.1

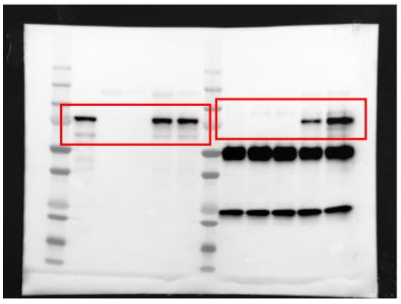

cMyc-RBP

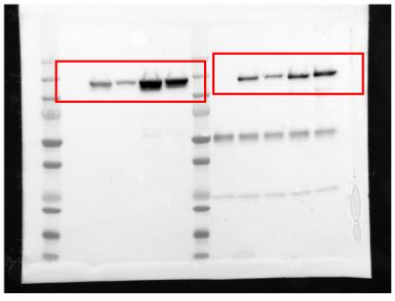

GAPDH